Figure S1. Characterization of intergenic transcripts. Related to Figure 3.

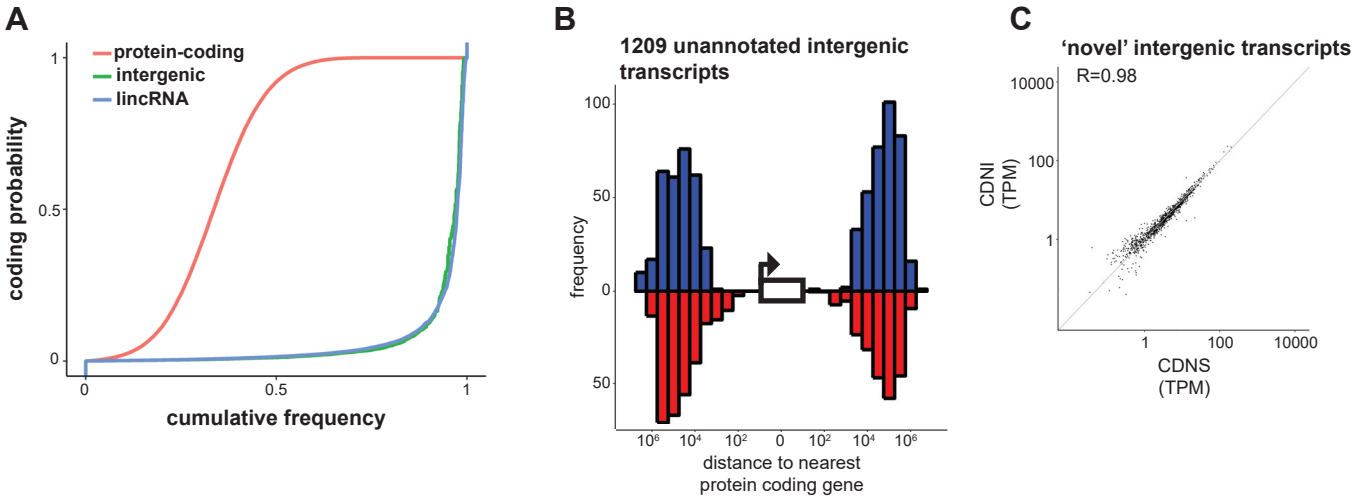

Figure S2. Introns are enriched in the CDNI scaffold. Related to Figure 3.

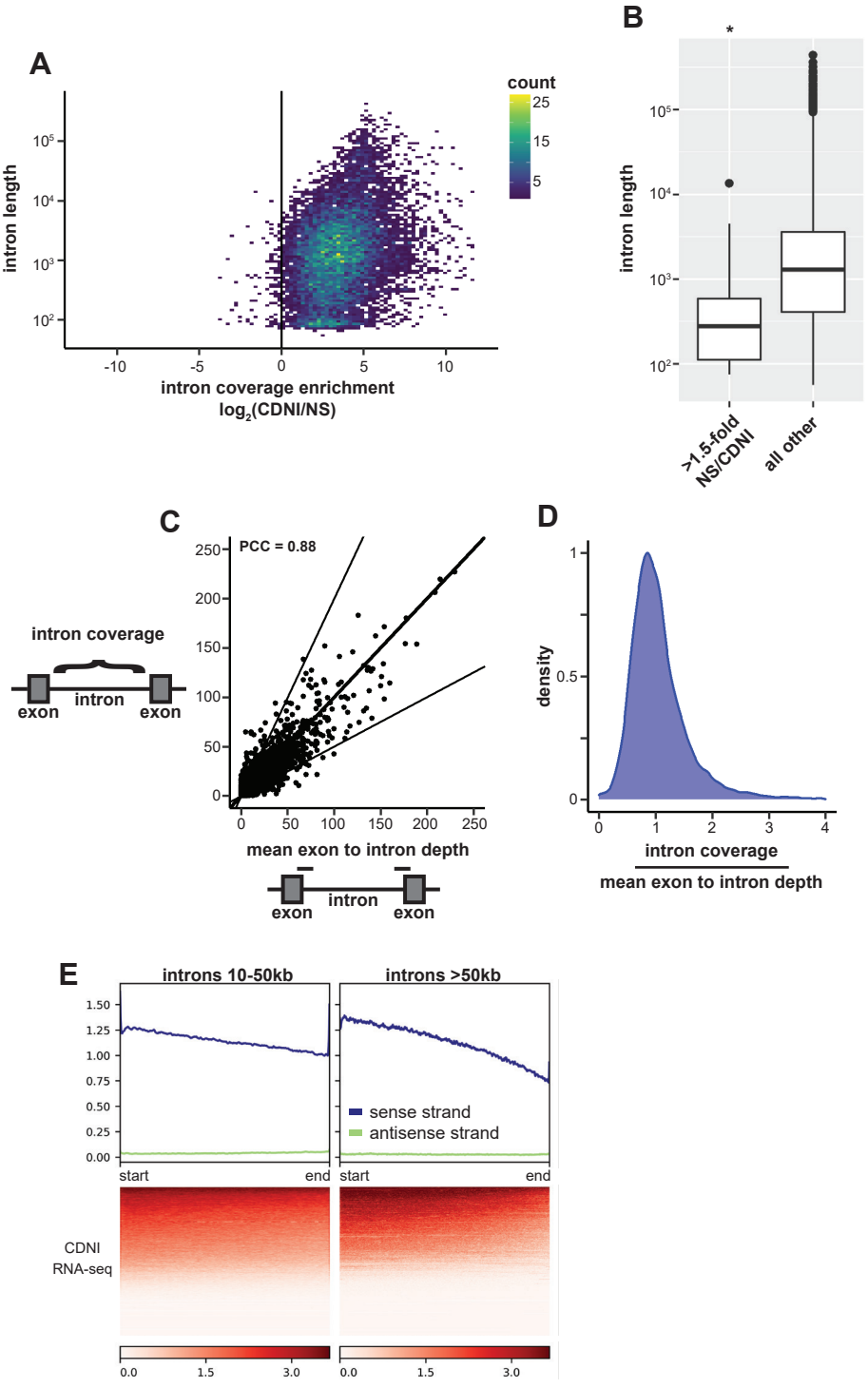

Figure S3. DRB can induce insoluble intergenic transcripts. Related to Figure 4.

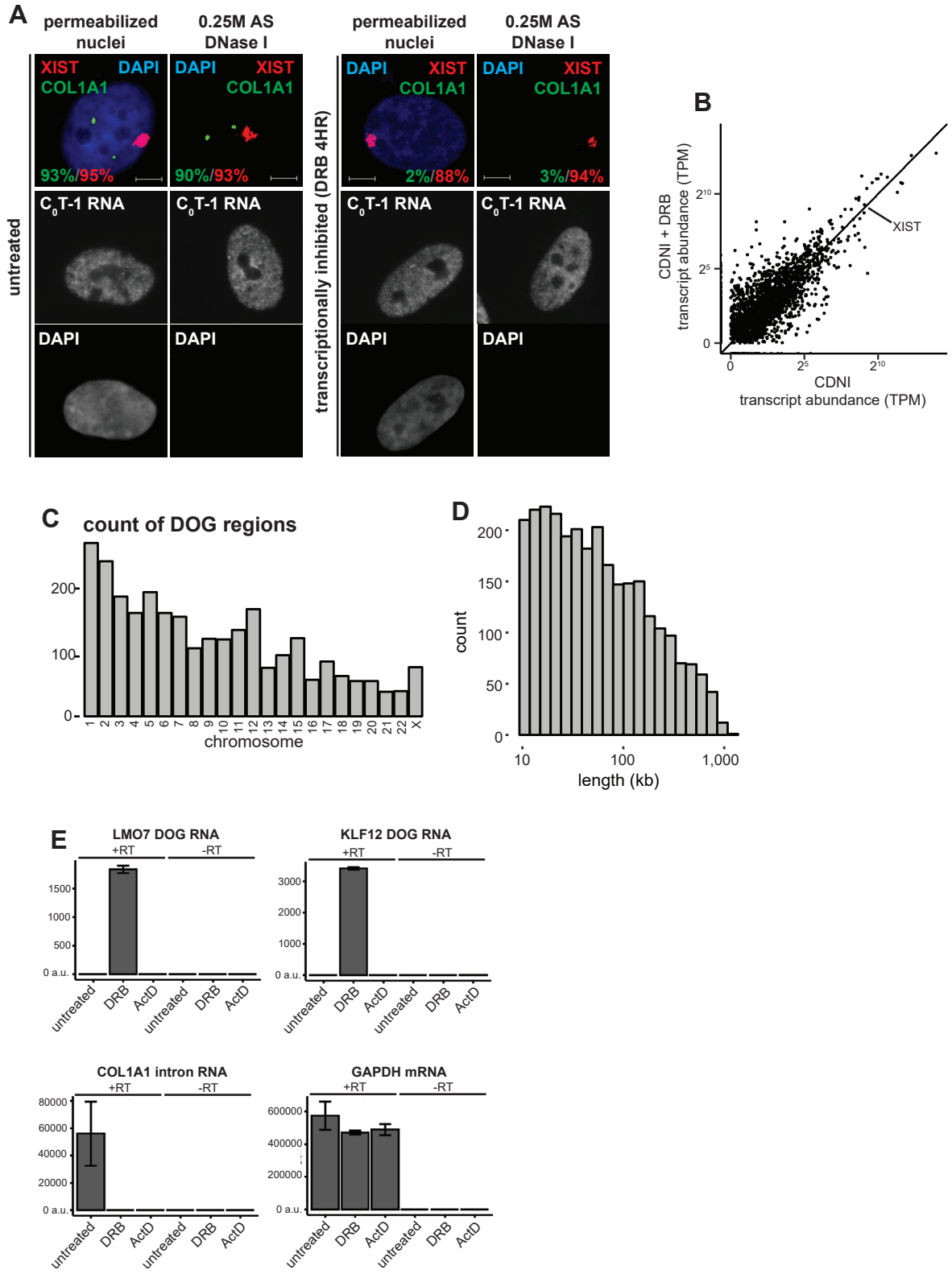

Figure S4. DNA distribution changes after co-treatment of cells with BAPTA-AM and DRB. Related to Figure 4.

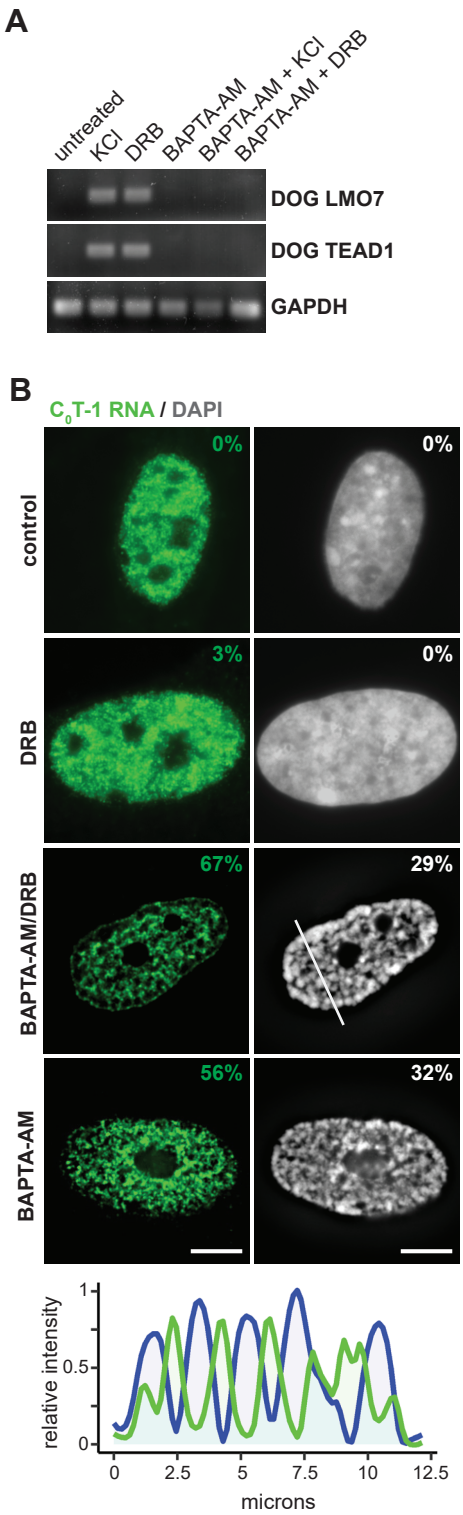

Figure S5. Specific nuclear scaffold proteins are enriched on euchromatin. Related to Figure 5.

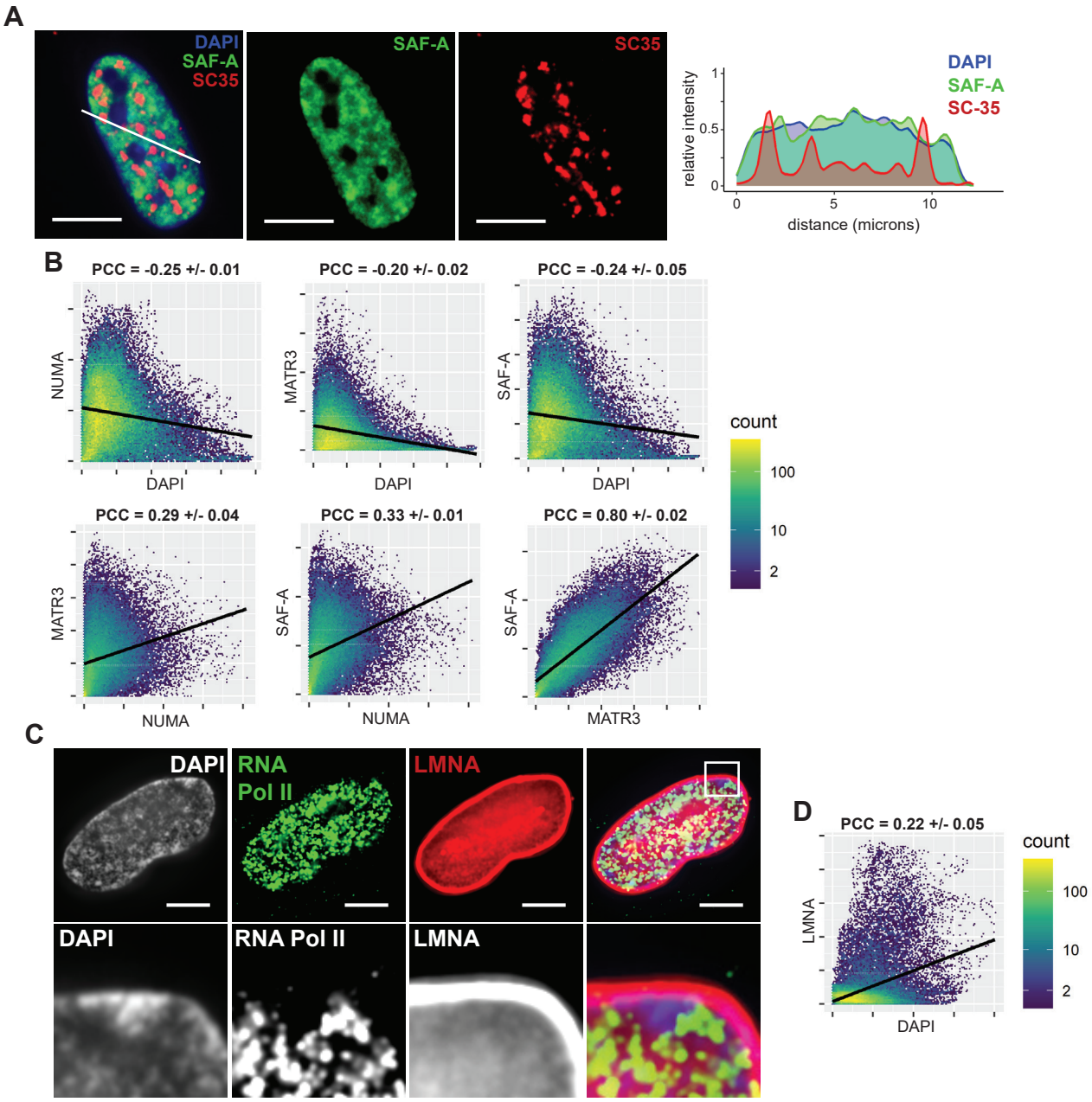

Figure S6. SAF-A and NUMA are depleted from compact chromatin after transcription arrest. Related to Figure 6.

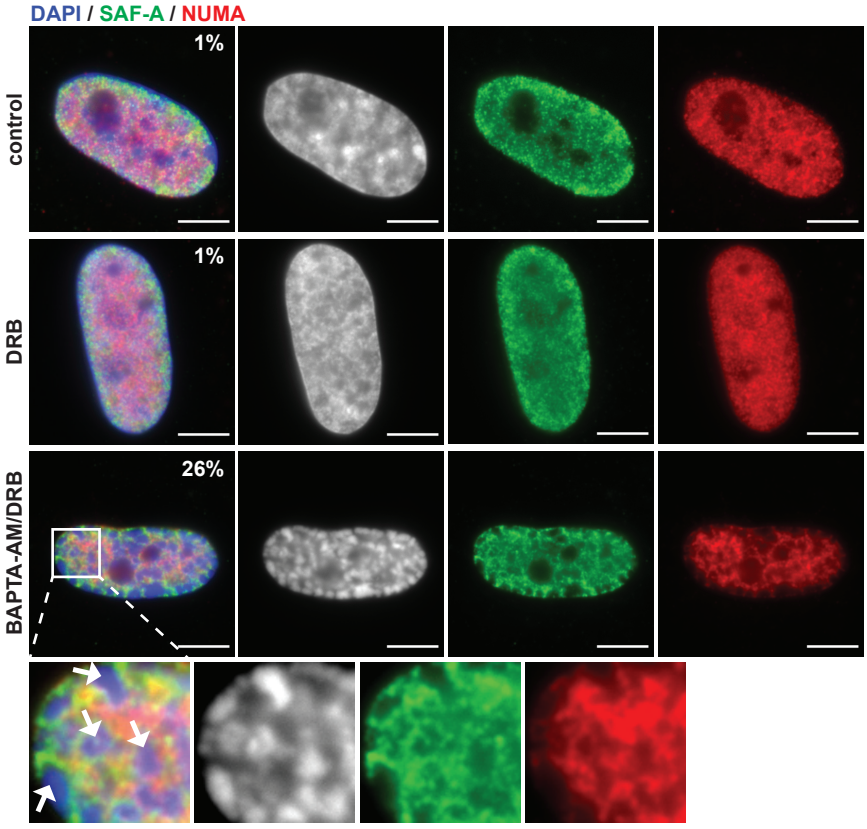

Figure S7. RNase depletes SAF-A from nuclei and SAR-seq enrichment in transcribed regions. Related to Figure 7.

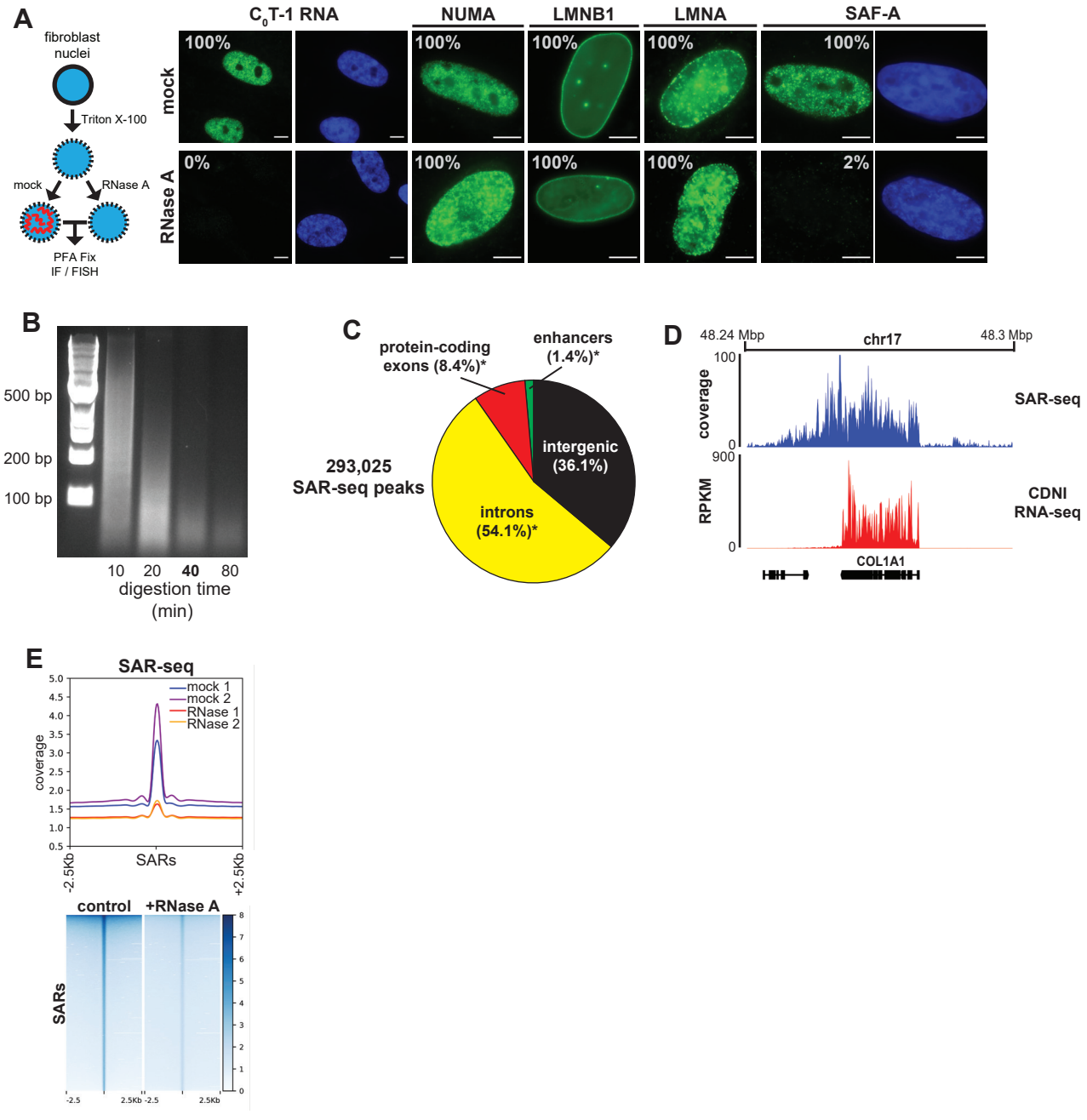

Table S1. Oligonucleotide primers used in this study. Related to Figure 4.

Oligonucleotides	SOURCE
RT-PCR primer, LMO7 DOG forward: ATTTGCCCATTGCCAGATAC	This paper
RT-PCR primer, LMO7 DOG reverse: CATGGATATGTCCCCTTCCA	This paper
RT-PCR primer, KLF12 DOG forward: TGACAAGCTGGTCTGGTGAG	This paper
RT-PCR primer, KLF12 DOG reverse: GAGGAAGCCCAATGTTGAAA	This paper
RT-PCR primer, TEAD1 DOG forward: GAAGGTGGATGCCAAGTGTT	This paper
RT-PCR primer, TEAD1 DOG reverse: ACAAGGCAGCATCTTTTGCT	This paper
RT-PCR primer, COL1A1 exon-spanning forward: GAGGGCCAAGACGAAGACATC	This paper
RT-PCR primer, COL1A1 exon-spanning reverse: CAGATCACGTCATCGCACAAC	This paper
RT-PCR primer, COL1A1 intron: GGGAATGGAAGGGAGATGAT	This paper
RT-PCR primer, COL1A1 intron: CTCTCTTGCACCAACTCACG	This paper
RT-PCR primer, GAPDH exon-spanning forward: TGCACCACCAACTGCTTAGC	This paper
RT-PCR primer, GAPDH exon-spanning reverse: GGCATGGACTGTGGTCATGAG	This paper

SUPPLEMENTAL FIGURE LEGENDS

Figure S1. Characterization of intergenic transcripts. Related to Figure 3. (A) Coding probability of GENCODE protein-coding and lincRNAs relative to 'novel' intergenic transcripts identified in this study. (B) Frequency of unannotated intergenic transcripts identified in this study relative to the location of their nearest protein coding gene. Forward strand transcripts relative to their nearest gene are indicated in blue and reverse in red. (C) Relative abundance of 'novel' intergenic transcripts in CDNI and CDNS fractions.

Figure S2. Introns are enriched in the CDNI scaffold. Related to Figure 3. (A) 2D Histogram of intron length (Y-axis) and $\log_2$ fold enrichment in the CDNI fraction (X-axis) for individual introns. (B) Boxplot of intron length distribution for introns enriched 1.5-fold in the NS fraction relative to the CDNI fraction and all other introns. Asterisk indicates statistical significance ($p<0.05$, Student's t-test). (C) Scatter plot of intron coverage (Y-axis) and unspliced junction read depth (X-axis) for individual introns in CDNI fraction RNA-seq. PCC, Pearson correlation coefficient. Lines are slope of 0.5,1, and 2. (D) Density plot of the ratio between intron coverage and mean unspliced junction read depth for introns in CDNI fraction RNA-seq. (E) Average coverage plot and heatmap of CDNI RNA-seq coverage at long (10-50kb, n=17,598) and very long (>50kb, n=3,656) Refseq select introns. Introns were scaled to 10kb in length for plotting. 50.0% of RNA-seq reads mapped entirely within long and very long introns in the CDNI fraction.

Figure S3. DRB can induce insoluble intergenic transcripts. Related to Figure 4. (A) RNA FISH analysis of untreated (left panels) or DRB-treated (4 hours) fibroblasts. Nuclei were permeabilized and either immediately fixed or extracted with 0.25M ammonium sulfate (AS) and DNase I-treated before fixation. The COL1A1 probe is BAC consisting mainly of COL1A1 intron. Scale bars 5 μm. (B) Scatter plot of GENCODE lncRNA abundance in the CDNI fraction of untreated or DRB-treated (4 hours) fibroblasts as determined by RNA-seq. (C) Histogram of DRB-induced downstream of gene (DOG) instances. (D) Histogram of contiguous DOG regions binned by length. (E) qRT-PCR analysis after treatment with DRB or Actinomycin D (ActD) for 6 hours. Reactions without reverse transcriptase (-RT) are included to account for potential DNA contamination. COL1A1 intron detected with primers in the 26th intron of the COL1A1 gene. GAPDH mRNA detected with exon-spanning primers. Error bars represent SEM (n=3). Unlike ActD, which intercalates into DNA and prevents RNA polymerase elongation, DRB is a less direct inhibitor of transcription that does not effectively inhibit already elongating polymerases (Gressel et al., 2017; Jonkers et al., 2014). In addition to blocking the transition from initiation to elongation, it is known that inhibition of CDK9, the target of DRB, can disrupt transcription termination (Sanso et al., 2016; Veloso et al., 2014). To our knowledge our study is the only one to detect widespread induction of intergenic transcription following DRB treatment, indicating induction of DOG transcripts may be cell-type or condition dependent. The varying degree of continued transcription and RNA retention in DRB treated cells may therefore explain the different impact of DRB on chromatin compaction observed by various labs.

Figure S4. DNA distribution changes after co-treatment of cells with BAPTA-AM and DRB. Related to Figure 4. (A) RT-PCR analysis of DOG transcripts on total RNA following osmotic stress (120 mM KCl, 2 hours), transcription inhibition (DRB, 4 hours), chelation of intracellular calcium (BAPTA-AM, 4 hours) or osmotic stress and transcription inhibition following pretreatment of media for 30 minutes with BAPTA-AM. (B) RNA FISH analysis of TIG-1 fibroblasts either mock treated, transcriptionally inhibited for 4 hours with DRB, or pre-treated with BAPTA-AM for 30 minutes prior to an additional 4 hour co-treatment with DRB.

Percentages indicate the number of cells with a large visual reduction in C_0T-1 RNA signal or dramatic chromatin collapse characterized by many DAPI-dense bodies as shown (n=100 for each condition). Scale bars 5 μm. A line-scan of C_0T-1 RNA and DAPI signal intensity for the indicate region is below. We often observed chromatin compaction observed similar changes when cells were treated with BAPTA-AM alone for extended periods, potentially related to prior observations of BAPTA-AM itself being a potent inhibitor of RNA synthesis (Shang and Lehrman, 2004).

Figure S5. Specific nuclear scaffold proteins are enriched on euchromatin. Related to Figure 5. (A) Immunofluorescence and accompanying line-scan of SAF-A and SC-35 localization in human fibroblasts. SAF-A is not enriched in SC-35 domains. Scale bars 5 μm. (B) Pixel intensity scatter plots for the nuclei shown in Figure 5A. Linear regression models are indicated by black lines. Pearson correlation coefficients were calculated independently for multiple nuclei and presented as the mean and 95% confidence interval for the mean of PCCs determined independently from four nuclei. (C) Immunofluorescence analysis of RNA Pol II and LMNA in fibroblasts. Magnified images of the indicated region are below. Scale bars 5 μm. (D) Pixel intensity scatter plots comparing LMNA and DAPI intensity in the nuclei shown in (C). PCC and 95% confidence intervals were calculated as above from four nuclei.

Figure S6. **SAF-A and NUMA are depleted from compact chromatin after transcription arrest. Related to Figure 6.** Immunofluorescence of TIG-1 fibroblasts either mock treated, transcriptionally inhibited for 4 hours with DRB, or pre-treated with BAPTA-AM for 30 minutes prior to an additional 4 hour co-treatment with DRB. Percentages indicate the number of cells with many DAPI-dense bodies (n=100 for each condition). Arrows in higher magnification images indicate regions of increased chromatin compaction. Scale bars 5 μm.

Figure S7. RNase depletes SAF-A from nuclei and SAR-seq enrichment in transcribed regions. Related to Figure 7. (A) Immunofluorescence or RNA FISH analysis as indicated of permeabilized nuclei either mock or RNase-treated for 10 minutes at 37°C prior to fixation. Equivalent exposures were used for comparisons. Percentages indicate interphase nuclei scored for clear nuclear signal for each RNA/protein following mock or RNase treatment (n=50). (B) Agarose gel electrophoresis analysis of DNA size after the DNase I digestion step of SAR-seq. The 40 minute time point was used for SAR isolation and sequencing. Samples sent for sequencing were 95-97% digested by mass. (C) Pie chart of the percentage of SAR-seq peaks that intersect with indicate regions of the genome. Asterisks indicate higher frequency of SAR-seq peaks in each region as determined by Genome Association Tester ($p<0.001$). SAR-seq peaks were found at lower frequency than expected in intergenic regions ($p<0.001$). (D) Coverage map of SAR-seq and CDNI RNA-seq at the COL1A1 gene and surrounding regions. (E) Heatmap (average of replicates) and average coverage profile for independent replicates of SAR-seq at SAR-seq peaks (+/- 5 Kb).